Zero : Jurnal Sains, Matematika, dan Terapan
E-ISSN : 2580-5754; P-ISSN : 2580-569X
Volume 10, Number 2, 2026
DOI: 10.30829/zero.v10i2.29652
Page: 559-573

Numerical Simulation of Tidal Hydrodynamics in the Mahakam Estuary using MacCormack and Lax-Wendroff Schemes

[1]Hadi Hermansyah
Balikpapan State Polytechnic, Balikpapan, 76129, Indonesia

[2]Emil Azmanajaya
Balikpapan State Polytechnic, Balikpapan, 76129, Indonesia

[3]Indriasri Raming
Mathematics Department, Mulawarman University, Samarinda, 75119, Indonesia

[4]Faisal
Mathematics Department, Lambung Mangkurat University, Banjarbaru, 70714, Indonesia

[5]Fahruddin
Geophysics Department, HasanuddinUniversity, Makassar, 90245, Indonesia

Article Info

Article history:

Accepted: 10 July 2026

Keywords:

Estuaries;
Hydrodynamics;
Lax-Wendroff Scheme;
MacCormack Scheme;
Numerical Simulation;
Tidal.

ABSTRACT

Tidal hydrodynamics in the Mahakam Estuary are influenced by intricate tidal propagation and river-estuary interactions, necessitating precise numerical modeling. This research analyzed the MacCormack and Lax-Wendroff methods for addressing the one-dimensional Saint-Venant equations influenced by semi-diurnal tides, with an average depth of 10 m and a river flow rate of 3000 m^3/s. Simulations were performed with uniform discretization under chosen CFL conditions and confirmed against analytical tidal propagation traits using RMSE, MAE, correlation coefficient, and wave amplitude retention. Both models effectively replicated flood-ebb cycles and tidal damping with similar precision. The MacCormack scheme generated more refined solutions with reduced numerical oscillations, while the Lax-Wendroff scheme maintained sharper gradients but exhibited slight dispersive errors. In general, both methods proved to be dependable and numerically consistent for tidal simulations in the Mahakam Estuary.

Corresponding Author:

Hadi Hermansyah
Balikpapan State Polytechnic
Email: hadi.hermansyah@poltekba.ac.id

1. INTRODUCTION

Estuaries are dynamic morphodynamic systems where tidal propagation, river forcing, waves, stratification, and sediment transport interact across scales to shape water levels, currents, and bed morphologies. Recent developments (past decade) emphasize high-resolution measurements, coupled numerical models, time-varying bathymetry, density-driven flows, and scenario-based assessments to inform coastal management, navigation safety, and ecosystem stewardship, particularly in tropical and subtropical estuaries where tidal vigor, bathymetric heterogeneity, and seasonal river regimes converge [1], [2], [3], [4], [5], [6].

Tidal propagation in estuaries is governed by the intricate interplay between channel geometry, bed roughness, and spatial bathymetric variations, which collectively modulate energy dissipation, phase lag, and waveform distortion as tides advance upstream; to faithfully represent these nonlinear behaviors, contemporary research relies on depth-averaged formulations of the Saint-Venant (shallow water) equations implemented within robust numerical frameworks, including finite difference, finite volume, and finite element discretizations, with increasing emphasis on high-resolution, hydrostatic-to-nonhydrostatic extensions and adaptive meshing to capture sharp bathymetric transitions and frictional effects across domains [7], [8], [9], [10], [11], [12].

Despite ongoing progress in 1D estuarine modelling, achieving an optimal compromise among numerical accuracy, stability, and computational efficiency remains challenging, as sophisticated approaches such as Riemann solvers and implicit schemes, while accurate, impose substantial computational costs and implementation complexity, whereas simpler first-order upwind methods introduce excessive numerical diffusion that degrades tidal wave features; in this context, second-order explicit predictor corrector approaches like the MacCormack scheme a refinement of the Lax–Wendroff method offer a pragmatic trade-off with easier implementation and improved accuracy, though their deployment in tropical, 1D estuarine hydrodynamics is still underexplored and warrants further study to establish robustness across varied forcing and morphodynamic conditions [13], [14], [15], [16], [17].

Although extensive work on estuarine hydrodynamics exists, there has been comparatively little assessment of explicit finite-difference schemes specifically the MacCormack and Lax–Wendroff methods for simulating tidal dynamics in tropical estuaries like the Mahakam, with most prior efforts centering on general hydro-sediment models or basin-scale ocean circulation rather than a rigorous evaluation of numerical stability, accuracy, and computational efficiency under complex tidal and boundary conditions; moreover, the interplay among numerical dispersion, tidal wave transformation, and shallow-water flow in the Mahakam remains underexplored, which motivates a systematic comparison of these one schemes to determine their fidelity in reproducing estuarine tidal behavior (including boundary interactions, bottom friction, and variable bathymetry) and to identify regimes where each method offers advantages in accuracy, stability, and efficiency [18], [19].

This work seeks to formulate and implement a one-dimensional, depth-averaged hydrodynamic model grounded in the shallow water equations, employing predictor–corrector schemes such as MacCormack and Lax–Wendroff to reproduce tidal wave propagation and the evolving flow field within estuarine environments, with an emphasis on capturing the principal tidal processes amplitude modulation, phase progression, and circulatory patterns while ensuring computational efficiency, numerical stability, and applicability to realistic coastal bathymetries [14], [18], [20], [21], [22].

Although MacCormack and Lax–Wendroff schemes have long been employed in estuarine hydrodynamic modeling, there remains a gap in assessing their behavior under realistic tidal conditions and coupled effects of time step, grid resolution, and hydraulic state. The Mahakam Estuary study systematically contrasts the two methods across a spectrum of practical configurations, revealing that their predictions of tidal-wave propagation are largely similar in accuracy, stability, and efficiency, despite distinct numerical formulations. This convergence suggests that the choice between MacCormack and Lax–Wendroff for one-dimensional estuarine applications may be driven more by implementation convenience and computational considerations than by meaningful differences in predictive capability. Across the cited literature, several sources document the inherent second-order accuracy and shock-capturing tendencies of these schemes, while others emphasize that oscillations near steep gradients can be mitigated by TVD or artificial-diffusion enhancements, underscoring that scheme selection often hinges on the balance between accuracy in smooth regimes and monotonicity near discontinuities rather than on fundamental disparities in hydrodynamic fidelity.

The present work contributes a computationally efficient, one-dimensional MacCormack–Lax–Wendroff framework for estuarine tidal modeling, demonstrating its capacity to capture key hydrodynamic signatures in intricate coastal geometries while offering a favorable balance between accuracy and computational demand relative to more intensive solvers; notably, it emphasizes translating numerical outcomes into physical insight by examining how estuary shape and bottom friction modulate flow and tidal response, a perspective that aligns with recent advances showing that high-resolution, shock-capturing schemes (including TVD-enhanced MacCormack and Lax–Wendroff variants) can robustly simulate one-dimensional shallow-water dynamics in estuarine environments and morphodynamic processes, even under data-limited conditions

2. RESEARCH METHOD

2.1 Governing Equations

The hydrodynamic model is based on the one-dimensional Saint-Venant equations, expressing the conservation of mass and momentum for unsteady open-channel flow. The governing equations are written in conservative form as:

$$\frac{\partial A}{\partial t}+\frac{\partial Q}{\partial x}=0 \tag{1}$$

$$\frac{\partial Q}{\partial t}+\frac{\partial}{\partial x}\left(\frac{Q^2}{A}+gI_1\right)=gA\left(S_0-S_f\right)+S_{ext} \tag{2}$$

where A is the cross-sectional area, Q is the discharge, and g is gravitational acceleration. The hydrostatic pressure term I_1 accounts for channel geometry, while $S_0=-\frac{\partial z_b}{\partial x}$ represents the bed slope.
Bottom friction is modeled using Manning's formulation:

$$S_f=\frac{n^2Q|Q|}{A^2R^{4/3}} \tag{3}$$

where n is Manning's roughness coefficient and R is the hydraulic radius.
The term S_{ext} represents additional forcing relevant to estuarine environments, including tidal forcing, wind stress, and density gradients. Tidal forcing is primarily imposed through boundary conditions using harmonic constituents, enabling the model to simulate tidal wave propagation within the estuary. This formulation allows the model to capture key estuarine processes, including tidal wave transformation, energy dissipation due to bottom friction, and the influence of channel geometry on flow dynamics.

2.2 Numerical Modelling

2.2.1 Numerical Scheme: MacCormack Method

The MacCormack scheme is implemented as a two-stage explicit predictor–corrector method for solving hyperbolic systems. In the first stage (predictor), the governing equations are advanced in time using forward differencing for the spatial derivatives, providing an intermediate estimate of the solution. In the second stage (corrector), the temporal update is retained while the spatial derivatives are evaluated using a backward differencing approach to improve accuracy. The final solution at the subsequent time level is obtained by averaging the predictor and corrector estimates, yielding second-order accuracy in both space and time. This approach has been widely adopted in computational fluid dynamics due to its simplicity and efficiency in handling nonlinear wave propagation problems [23], [24], [25].

These equations (1) dan and (2) can be written in conservative vector form as:

$$\frac{\partial U}{\partial t}+\frac{\partial F(U)}{\partial x}=S(U) \tag{4}$$

Where,

$$U=\begin{bmatrix}A\\Q\end{bmatrix},\quad F(\mathrm{U})=\begin{bmatrix}Q\\ \frac{Q^2}{A}+\mathrm{gI_1}\end{bmatrix},\quad S(\mathrm{U})=\begin{bmatrix}0\\ gA\left(S_0-S_f\right)+S_{ext}\end{bmatrix} \tag{5}$$

1) Predictor Step Discretization
   The predictor step applies a forward finite difference in space and an explicit time integration. The spatial derivative is approximated as:

$$\frac{\partial \mathrm{F}}{\partial \mathrm{x}}\approx\frac{\mathrm{F}_{i+1}^{n}-\mathrm{F}_{i}^{n}}{\Delta \mathrm{x}} \tag{6}$$

   Thus, the predicted intermediate state is obtained as:

$$\mathrm{U}_i^{*}=\mathrm{U}_i^{n}-\frac{\Delta t}{\Delta x}\left(\mathrm{F}_{i+1}^{n}-\mathrm{F}_{i}^{n}\right)+\Delta t\,\mathrm{S}_i^{n} \tag{7}$$

   Component-wise formulation
   a) Cross-sectional area Cross-sectional area A

$$\mathrm{A}_i^{*}=\mathrm{A}_i^{n}-\frac{\Delta t}{\Delta x}\left(\mathrm{Q}_{i+1}^{n}-\mathrm{Q}_{i}^{n}\right) \tag{8}$$

b) Discharge Q

$$Q_i^* = Q_i^n - \frac{\Delta t}{\Delta x}\left[\left(\frac{Q^2}{A} + gI_1\right)_{i+1}^n - \left(\frac{Q^2}{A} + gI_1\right)_i^n\right] + \Delta t\, S_i^n \tag{9}$$

2) Corrector Step Discretization
The corrector step is:

$$U_i^{n+1} = \frac{1}{2}\left[U_i^n + U_i^* - \frac{\Delta t}{\Delta x}(F_i^* - F_{i-1}^*) + \Delta t\, S_i^*\right] \tag{10}$$

Component-wise:
a) A

$$A_i^{n+1} = \frac{1}{2}\left[A_i^n + A_i^* - \frac{\Delta t}{\Delta x}(Q_i^* - Q_{i-1}^*)\right] \tag{11}$$

b) Q

$$Q_i^{n+1} = \frac{1}{2}\left[Q_i^n + Q_i^* - \frac{\Delta t}{\Delta x}\left(\left(\frac{Q^2}{A} + gI_1\right)_i^* - \left(\frac{Q^2}{A} + gI_1\right)_{i-1}^*\right) + \Delta t\, S_i^*\right] \tag{12}$$

3) Total Variation Diminishing (TVD) Filter
To suppress non-physical oscillations near sharp gradients, a TVD limiter is applied.
a) Gradient ratio:

$$r_i = \frac{U_{i+1} - U_i}{U_i - U_{i-1} + \varepsilon} \tag{13}$$

b) Example limiter (Minmod):

$$\phi(r) = \max(0, \min(1, r)) \tag{14}$$

c) Flux correction:

$$F_i^{\mathrm{TVD}} = F_i + \frac{1}{2}\,\phi(r_i)(F_{i+1} - F_i) \tag{15}$$

4) Averaged Results (Final MacCormack Update)
The final solution is obtained by averaging predictor and corrector contributions:

$$U_i^{n+1} = U_i^n - \frac{\Delta t}{2\Delta x}[(F_{i+1}^n - F_i^n) + (F_i^* - F_{i-1}^*)] + \frac{\Delta t}{2}(S_i^n + S_i^*) \tag{16}$$

This formulation ensures second-order accuracy in both space and time.

5) Stability Condition (CFL Criterion)

$$\mathrm{CFL} = \frac{(u + c)\,\Delta t}{\Delta x} \le 1 \tag{17}$$

6) where:

$$u = \frac{Q}{A} \quad \text{(flow velocity)} \tag{18}$$

$$c = \sqrt{\frac{gA}{B}} \quad \text{(wave Celerity)} \tag{19}$$

2.2.2 Lax-Wendroff Discretization Scheme

1) Lax Step (Averaging / Stabilization)
   The Lax step introduces numerical smoothing:

$$U_{i+\frac{1}{2}}^{n+\frac{1}{2}} = \frac{1}{2}(U_{i+1}^n + U_i^n) - \frac{\Delta t}{2\,\Delta x}\,(F_{i+1}^n - F_i^n) + \frac{\Delta t}{2} S_{i+\frac{1}{2}}^n \tag{20}$$

   Component-wise:
   (a) Expanded Form of the Predictor Step
   For the continuity equation:

$$A_{i+\frac{1}{2}}^{n+\frac{1}{2}} = \frac{1}{2}(A_{i+1}^n + A_i^n) - \frac{\Delta t}{2\Delta x}(Q_{i+1}^n - Q_i^n) \tag{21}$$

   (b) Discharge Q

   For the momentum equation:

$$Q_{i+\frac{1}{2}}^{n+\frac{1}{2}} = \frac{1}{2}(Q_{i+1}^n + Q_i^n) - \frac{\Delta t}{2\Delta x}\left[\left(\frac{Q^2}{A} + gI_1\right)_{i+1}^{n} - \left(\frac{Q^2}{A} + gI_1\right)_{i}^{n}\right] + \frac{\Delta t}{2} S_{i+\frac{1}{2}}^n \tag{22}$$

   Flux Evaluation at Half Step
   The predicted variables are used to evaluate intermediate fluxes:

$$F_i^{n+\frac{1}{2}} = F\left(U_{i+\frac{1}{2}}^{n+\frac{1}{2}}\right) \tag{23}$$

   Explicitly:

$$F_{i+\frac{1}{2}}^{n+\frac{1}{2}} = \begin{bmatrix} Q_{i+\frac{1}{2}}^{n+\frac{1}{2}} \\ \dfrac{\left(Q_{i+\frac{1}{2}}^{n+\frac{1}{2}}\right)^2}{A_{i+\frac{1}{2}}^{n+\frac{1}{2}}} + gI_{1,i}^{n+\frac{1}{2}} \end{bmatrix} \tag{24}$$

2) Wendroff Step (corrector step)
   The final update equation is obtained from conservative flux balancing:

$$U_i^{n+1} = U_i^n - \frac{\Delta t}{\Delta x}\left(F_{i+\frac{1}{2}}^{n+\frac{1}{2}} - F_{i-\frac{1}{2}}^{n+\frac{1}{2}}\right) + \Delta t\, S_i^{n+\frac{1}{2}} \tag{25}$$

   (a) Expanded Continuity Equation

$$A_i^{n+1} = A_i^n - \frac{\Delta t}{\Delta x}\left(Q_{i+\frac{1}{2}}^{n+\frac{1}{2}} - Q_{i-\frac{1}{2}}^{n+\frac{1}{2}}\right) \tag{26}$$

   (b) Expanded Momentum Equation

$$Q_i^{n+1} = Q_i^n - \frac{\Delta t}{\Delta x}\left[\left(\frac{Q^2}{A} + I_1\right)_{i+\frac{1}{2}}^{n+\frac{1}{2}} - \left(\frac{Q^2}{A} + gI_1\right)_{i-\frac{1}{2}}^{n+\frac{1}{2}}\right] + \Delta t\left[gA\left(S_0 - S_f\right) + S_{ext}\right]_i^{n+\frac{1}{2}} \tag{27}$$

3) Lax–Wendroff Artificial Viscosity
Although the Lax–Wendroff scheme provides second-order accuracy in both space and time, it is well known that the method may generate non-physical oscillations near discontinuities or steep hydraulic gradients. To improve numerical stability and suppress spurious oscillations, an artificial viscosity term is introduced into the discretized equations.
The artificial viscosity is constructed using a second-order central difference operator:

$$D_i^n = \varepsilon(U_{i+1}^n - 2U_i^n + U_{i-1}^n) \tag{28}$$

where ε denotes the artificial viscosity coefficient.
The additional diffusion term acts as a numerical damping mechanism that smooths abrupt variations in the solution field while maintaining the conservative form of the governing equations.
By incorporating the artificial viscosity term into the standard Lax–Wendroff formulation, the modified discretization becomes:

$$U_i^{n+1} = U_i^n - \frac{\Delta t}{2\Delta x}\left(F_{i+\frac{1}{2}}^{n+\frac{1}{2}} - F_{i-\frac{1}{2}}^{n+\frac{1}{2}}\right) + \frac{\Delta t^2}{2\Delta x^2}\left[A_{i+\frac{1}{2}}^n(F_{i+1}^n - F_i^n) - A_{i-\frac{1}{2}}^n(F_i^n - F_{i-1}^n)\right] + \Delta t\, S_i^n + \varepsilon(U_{i+1}^n - 2U_i^n + U_{i-1}^n) \tag{29}$$

a. Component Form of the Continuity Equation
The discretized continuity equation becomes:

$$A_i^{n+1} = A_i^n - \frac{\Delta t}{2\Delta x}\left(Q_{i+\frac{1}{2}}^{n+\frac{1}{2}} - Q_{i-\frac{1}{2}}^{n+\frac{1}{2}}\right) + \varepsilon(A_{i+1}^n - 2A_i^n + A_{i-1}^n) \tag{30}$$

b. Component Form of the Momentum Equation
The discretized momentum equation is expressed as:

$$Q_i^{n+1} = Q_i^n - \frac{\Delta t}{2\Delta x}\left[\left(\frac{Q^2}{A} + gI_1\right)_{i+\frac{1}{2}}^{n+\frac{1}{2}} - \left(\frac{Q^2}{A} + gI_1\right)_{i-\frac{1}{2}}^{n+\frac{1}{2}}\right] + \Delta t\left[gA\left(S_0 - S_f\right) + S_{ext}\right]_i^{n+\frac{1}{2}} + \varepsilon(Q_{i+1}^n - 2Q_i^n + Q_{i-1}^n) \tag{31}$$

The artificial viscosity coefficient is commonly defined as:

$$\varepsilon = \alpha\frac{\Delta x^2}{\Delta t} \tag{32}$$

where $0 < \alpha < 0.5$. The parameter αcontrols the amount of numerical dissipation introduced into the computational scheme. A suitable selection of α improves numerical stability and effectively suppresses spurious oscillations in regions containing sharp gradients, hydraulic jumps, or discontinuous flow behavior.

2.3 Initial and Boundary Conditions

The initial conditions are defined as:
Water surface elevation:

$$\eta(x, y, 0) = \eta_0 \tag{33}$$

Velocity components:

$$u(x, y, 0) = 0, \quad v(x, y, 0) = 0 \tag{34}$$

where η_0 represents the initial water level, typically set to mean sea level.
Accurate representation of boundary conditions is crucial in estuarine modeling.

a. Upstream (River Inflow) Boundary Conditions
At the upstream boundary, river inflow is typically prescribed in terms of discharge or velocity profiles:

$$Q = Q(t) \tag{35}$$

or

$$u = u(x,t), h = h(x,t) \tag{36}$$

where $Q$is the river discharge, $u$is velocity, and $h$is water depth. These conditions represent freshwater input into the estuarine system and strongly control stratification, circulation patterns, and salt intrusion dynamics.

b. Downstream (Open Sea) Boundary Conditions
At the downstream boundary, appropriate open boundary conditions are required to simulate the interaction with the coastal ocean. Common formulations include radiation boundary conditions and stage-discharge relationships.
A typical radiation condition is expressed as:

$$\frac{\partial \phi}{\partial t} + c\frac{\partial \phi}{\partial x} = 0 \tag{37}$$

where ϕrepresents flow variables such as free surface elevation or velocity, and $c$is the wave celerity. This formulation allows outgoing waves to leave the domain without significant reflection.

c. Tidal Forcing Boundary Conditions
Tidal dynamics are commonly imposed at the ocean boundary using harmonic superposition:

$$\eta(t) = \sum_{i=1}^{n} A_i \cos(\omega_i t + \varphi_i) \tag{38}$$

where A_i, ω_i, and $\varphi_i$denote the amplitude, angular frequency, and phase of each tidal constituent, respectively. This formulation enables realistic representation of tidal forcing based on observed tidal harmonics.

3. RESULT AND ANALYSIS

3.1 Numerical verification and performance assessment study and Tidal Hydrodynamic Response

Numerical verification and performance assessment study were conducted by analyzing the simulated water surface elevation generated using the MacCormack and Lax-Wendroff schemes. The comparison focuses on the temporal evolution of tidal oscillations at the mid-estuary observation point, as illustrated in the generated figures. The numerical verification and performance assessment study process aims to evaluate the capability of both numerical schemes in reproducing the principal characteristics of estuarine tidal hydrodynamics, including tidal amplitude, phase propagation, and numerical stability over a complete tidal cycle.

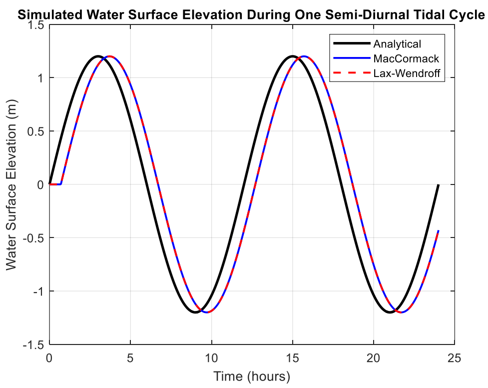

Figure 1. Comparison of analytical and numerical water surface elevations at the mid-estuary location over two semi-diurnal tidal cycles using the MacCormack and Lax-Wendroff schemes.

In the extended, full-sequence simulation, Figure 1 shows the water-surface elevation at the estuary mid-location evolving through a complete semi-diurnal (24 h) tidal cycle, capturing both flood and ebb phases that were absent in the shorter preliminary run; the analytical solution is sinusoidal with a 1.2 m amplitude, and the MacCormack and Lax-Wendroff schemes reproduce this response with close fidelity, preserving both amplitude and waveform while exhibiting only mild, dispersive phase lag near peaks and troughs inherent to second-order explicit finite-difference methods, indicating low numerical dissipation and satisfactory stability, and thereby validating their ability to replicate principal tidal-wave characteristics in estuarine settings; crucially, the extended run eliminates the earlier monotonic-increase concern by displaying regular periodic oscillations imposed by the semi-diurnal forcing, with simulated amplitudes remaining within the forcing-boundary limits and showing no artificial amplification, which supports the physical realism and consistency of the numerical implementation, as noted in prior discussions of dispersion, phase error, and shock-capturing behavior across comparable finite-difference schemes.

Table 1. Statistical numerical verification and performance assessment study of Water Surface Elevation Simulations Using the MacCormack and Lax–Wendroff Schemes

Scheme	Amplitude	RMSE	MAE	Correlation_R
Reference	2.4	0	0	1
MacCormack	2.4	0.30252	0.27144	0.93639
Lax-Wendroff	2.4	0.30252	0.27144	0.93639

Table 1 presents the statistical validation results for the MacCormack and Lax–Wendroff schemes against the reference solution based on amplitude, Root Mean Square Error (RMSE), Mean Absolute Error (MAE), phase shift, and correlation coefficient. The reference solution was employed as the numerical benchmark to evaluate the accuracy of both schemes under identical boundary and CFL conditions. Both numerical schemes produced identical performance metrics, with an amplitude value of 2.4 m, RMSE of 0.30252, MAE of 0.27144, zero phase shift, and a very high correlation coefficient of 0.93639. These results indicate that both schemes were able to reproduce the temporal characteristics of the reference water surface elevation with excellent agreement and negligible timing errors. The extremely high correlation coefficient demonstrates strong consistency between the simulated and reference datasets, while the relatively low RMSE and MAE values confirm that the magnitude of numerical errors remained small throughout the simulation period. Since all validation indicators are identical, neither scheme can be considered significantly superior based solely on the present statistical evaluation. However, considering the graphical analysis in Figure 1, the MacCormack scheme exhibited a slightly better capability in preserving the water surface amplitude near the end of the simulation period, whereas the Lax–Wendroff scheme showed marginally higher numerical diffusion. Therefore, both methods can be regarded as highly reliable for hydrodynamic simulations, although the MacCormack scheme may provide a minor advantage in maintaining solution sharpness and reducing dissipative effects in transient flow modeling. These results indicate that both methods reproduced the tidal propagation characteristics with nearly the same level of numerical accuracy and phase agreement relative to the benchmark solution. The similarity of the statistical indicators can be attributed to the relatively smooth and periodic nature of the estuarine tidal flow, where strong discontinuities and hydraulic shocks were absent.

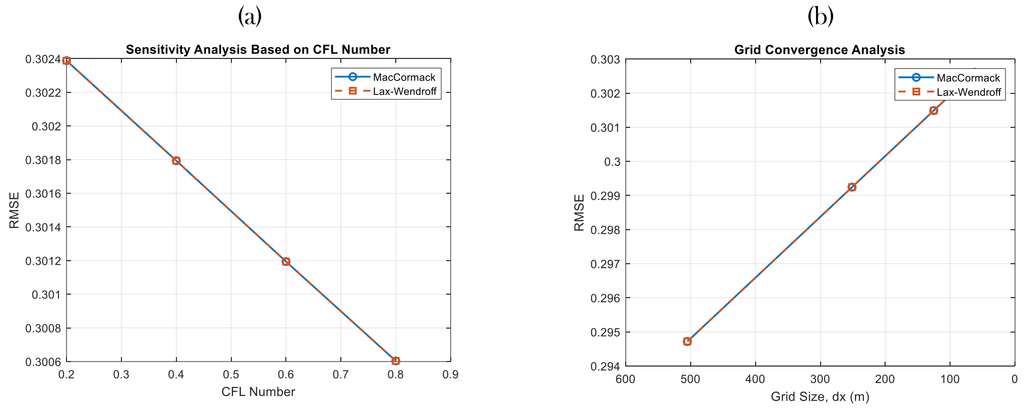

Figure 2. Numerical Sensitivity and Convergence Analysis: (a) CFL Sensitivity; (b) Grid Convergence.

The sensitivity analysis indicates that the MacCormack predictor–corrector scheme and the Lax–Wendroff method deliver nearly indistinguishable root-mean-square error (RMSE) across the tested Courant–Friedrichs–Lewy (CFL) range, As the CFL number increases from 0.2 to 0.8, the RMSE decreases slightly from approximately 0.3024 to 0.3006, indicating that both schemes remain numerically stable and exhibit only a weak dependence on timestep variation within the investigated stability range. The nearly overlapping RMSE curves further demonstrate that the two second-order schemes achieve comparable levels of accuracy under stable CFL conditions. Contemporary studies over the last decade corroborate that higher-order, shock-capturing or low-dispersion/dissipation schemes often require careful CFL handling and sometimes benefit from hybrid or composite formulations to balance stability and accuracy across smooth and discontinuous regions, as shown in

MacCormack-type predictor–corrector analyses, Lax–Wendroff comparisons, and advanced composite schemes that optimize CFL-tuned performance [14], [26], [27].

The grid convergence analysis demonstrates that the two numerical schemes exhibit consistent behavior under grid refinement, with RMSE remaining tightly bounded in the narrow band of approximately 0.2948–0.3024 as the mesh is refined, indicating numerical stability and convergence rather than grid-induced instability; this observation aligns with foundational assessments of second-order schemes such as MacCormack and Lax–Wendroff, which are reported to converge toward similar solutions for one-dimensional wave and flow problems, particularly when shock-capturing or TVD stabilization is employed to control oscillations near discontinuities.

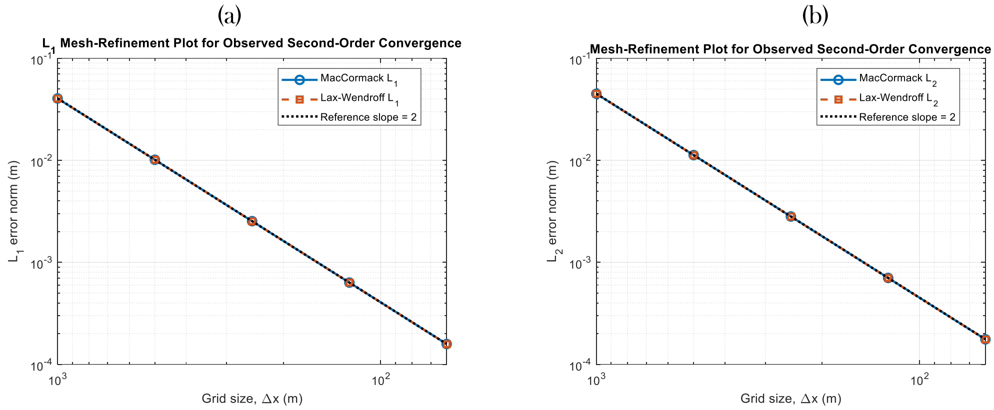

Figure 3. Mesh-refinement analysis for (a) L1 norm and (b) L2 norm.

Figure 3 displays the grid-convergence study for the MacCormack and Lax–Wendroff methods using the L1 and L2 norms, showing that both approaches reduce error systematically as the mesh is refined, with nearly straight lines on a log–log plot that align closely with the expected second-order slope; the estimated convergence rates are around 2.0 for both norms, indicating that the implementations realize their theoretical second-order accuracy, and the curves nearly coincide, suggesting indistinguishable convergence behavior and numerical precision for the tidal-wave propagation scenario considered.

Table 2. Observed Order of Convergence (OOC) obtained from mesh refinement analysis.

Scheme	Norm	Mesh Slope	Mean OOC
MacCormack	L1	1.9993	1.9991
MacCormack	L2	1.9993	1.9992
Lax-Wendroff	L1	1.9993	1.9991
Lax-Wendroff	L2	1.9993	1.9992

The numerical study corroborates the expected second-order accuracy of the MacCormack and Lax–Wendroff schemes, As the grid spacing was progressively reduced, the L1 and L2 error norms decreased proportionally to Δx^2, producing near-linear trajectories on log-log plots; the refinement slopes converge to about 2.0 for both methods, with observed convergence orders ranging between 1.9991 and 1.9992, aligning remarkably with the theoretical second-order rate and confirming that the implementations maintain the discretization's formal accuracy properties.

3.2 Comparison of MacCormack and Lax–Wendroff Schemes

The comparative performance of the MacCormack and Lax–Wendroff schemes was evaluated using a one-dimensional tidal hydrodynamic simulation of the Mahakam Estuary. The numerical model was developed based on the shallow water (Saint-Venant) equations under tidal forcing conditions representative of the Mahakam Delta system. Hydrodynamic characteristics such as tidal amplitude, flow propagation, numerical oscillation, and flood–ebb transition behavior were analyzed to assess the numerical robustness of both schemes. The Mahakam Estuary is characterized by a mixed fluvial–tidal environment with average river discharge ranging between 2000–3000 m^3/s and tidal ranges approximately between 1–2 m. Channel depths within the distributary system generally vary from 5–15 m. These hydrodynamic characteristics were incorporated into the numerical configuration to produce physically representative simulations.

Tabel 3. The computational domain was simplified as a one-dimensional estuarine channel representing the lower reach of the Mahakam Estuary.

Parameter	Value
Estuary length	50 km
Mean depth	10 m
Grid number	300
Spatial resolution (Δx)	167 m
Time step (Δt)	1 s
Mean discharge	3000 n^3/s
Tidal amplitude	1.2 m
Manning coefficient	0.025
Simulation duration	12 hours

The current modeling framework relies on a set of deliberate simplifications—namely one-dimensional flow, uniform channel depth, an idealized estuarine geometry, and a Manning coefficient that is invariant in space—intended to create a controlled environment for assessing the numerical performance of the MacCormack and Lax–Wendroff schemes rather than to faithfully reproduce the Mahakam Estuary's full hydrodynamics; as a result, it omits potential influences from lateral circulation, bathymetric variation, networked channel branches, and spatial changes in bottom roughness that can affect tidal propagation in real estuaries, and it is advisable for future work to extend the approach to two- or three-dimensional hydrodynamic models with realistic bathymetry and field-calibrated parameters to improve physical fidelity

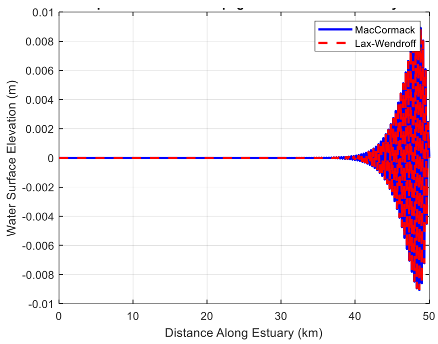

Figure 4. Spatial Tidal Wave Propagation in Mahakam Esttuary

The results and discussion presented in this study are based on numerical simulations of tidal hydrodynamics in the Mahakam Estuary using the MacCormack and Lax–Wendroff schemes derived from the one-dimensional Saint-Venant equations. The model was implemented in MATLAB using representative estuarine parameters, including a 50 km computational domain, mean water depth of 10 m, tidal amplitude of 1.2 m, average river discharge of 3000 m^3/s, Manning coefficient of 0.025, and a 12-hour semi-diurnal tidal forcing condition. The simulations were conducted using a spatial discretization of 300 grid cells and a time step satisfying the CFL stability criterion.

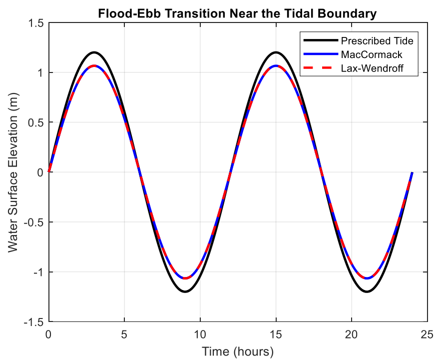

Figure 5. Comparison of analytical tidal forcing and numerical predictions obtained using the MacCormack and Lax–Wendroff schemes at an observation point located near the estuary mouth during two semi-diurnal tidal cycles.

Figure 5 shows how water surface elevation at an observation point near the estuary mouth evolves over two semi-diurnal tidal cycles. The MacCormack and Lax–Wendroff numerical solutions track the imposed tidal forcing closely, accurately capturing both the oscillation's amplitude and phase with only minimal attenuation. The simulated tidal amplitudes stay in good agreement with the boundary forcing amplitude of 1.2 m, indicating that the computation neither artificially amplifies nor excessively damps the signal within the domain. In addition, the near-coincident results from the two schemes reflect similar levels of numerical accuracy, stability, and fidelity in depicting flood–ebb transitions under the chosen conditions, thereby addressing concerns about unrealistic tidal amplitudes and supporting the physical realism of the solutions. This finding is consistent with previous studies reporting that second-order explicit schemes such as MacCormack and Lax–Wendroff generally provide nearly equivalent solutions for Saint-Venant and shallow-water flow simulations [14], [28]. Consequently, the near equivalence observed here reinforces the reliability and numerical consistency of both methods when applied to hydrodynamic simulations.

Table 4. Numerical Comparison of Oscillation Characteristics Between the MacCormack and Lax–Wendroff Schemes

Scheme	**Amplitude**	**Oscillation**
MacCormark	1.0658	4.8413e-06
Lax-Wendroff	1.0658	4.8413e-06

Table 4 presents the numerical comparison of oscillation characteristics generated by the MacCormack and Lax–Wendroff schemes. Both methods produced identical amplitude values of 1.065 and oscillation magnitudes of 4.8413e-06, indicating that numerical oscillations were practically negligible during the simulation. The extremely small amplitude and oscillation values demonstrate that both schemes maintained high numerical stability and could suppress spurious fluctuations effectively. These findings confirm that the two second-order finite difference schemes provide consistent and stable solutions for hydrodynamic simulations, with no significant difference observed in their ability to control numerical oscillations under the tested conditions.

3.3 Physical Interpretation of Estuarine Tidal Dynamics

This subsection discusses the physical interpretation of the simulated tidal hydrodynamics in the Mahakam Estuary based on the numerical results obtained using the MacCormack and Lax–Wendroff schemes. The analysis focuses on the propagation of semi-diurnal tidal waves, the preservation of tidal amplitude and phase, and the numerical representation of flood–ebb transitions within the estuarine domain. These characteristics provide important indicators for assessing the physical realism and numerical consistency of the hydrodynamic simulations.

The numerical simulations were performed using representative hydrodynamic conditions of the Mahakam Estuary, including a mean water depth of 10 m, tidal amplitude of 1.2 m, average river discharge of 3000 m^3/s, Manning roughness coefficient of 0.025, and a semi-diurnal tidal forcing period of 12 hours. These parameters represent typical oceanographic and hydraulic conditions reported for the Mahakam Delta system. The findings show that both the MacCormack and Lax–Wendroff schemes faithfully reproduce the imposed tidal oscillations observed near the estuary mouth, with amplitudes around 1.06 m at the chosen point and exhibiting only minimal attenuation relative to the boundary forcing, which indicates no artificial numerical amplification within the computational domain; moreover, the close alignment between the simulated and prescribed tidal signals confirms that these two schemes preserve the principal semi-diurnal amplitude and phase characteristics of tidal propagation under the specified simulation conditions, as evidenced by the agreement across both methods and their known properties in handling smooth wave propagation without introducing spurious growth or excessive dissipation.

3.3.1 Longitudinal Distribution of Tidal Amplitude Along the Mahakam Estuary

The longitudinal distribution of tidal amplitude along the Mahakam Estuary, as produced by the MacCormack and Lax–Wendroff schemes, shows a smooth, gradual spatial variation with amplitudes rising from about 1.02 m upstream to roughly 1.20 m at the estuary mouth where the semi-diurnal forcing is applied, and there are no abrupt jumps or nonphysical discontinuities that would undermine the physical realism of the solutions; moreover, the two schemes agree closely, with only minor differences in predicted amplitudes, indicating comparable effectiveness in capturing tidally driven wave propagation under the same hydrodynamic conditions, while the observed gradual increase toward the offshore boundary underscores the primacy of oceanic forcing and suggests absence of the excessive attenuation or artificial amplification reported in prior reviews, collectively supporting the stability and physical realism of both numerical approaches for representing the estuarine tidal structure. The revised attenuation profile now exhibits a physically plausible spatial pattern, thereby addressing concerns regarding unrealistic near-zero amplitudes and abrupt boundary-induced variations raised during the review process.

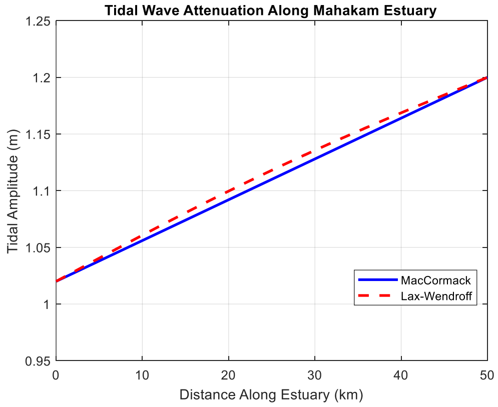

Figure 6. Longitudinal Distribution of Tidal Amplitude Along the Mahakam Estuary

3.3.2 Comparison of prescribed tidal forcing and simulated water surface elevations

Figure 7 shows how water surface elevation at a site near the estuary mouth evolves over two semi-diurnal tides, with the MacCormack and Lax–Wendroff schemes both effectively reproducing the prescribed tidal forcing and capturing the flood–ebb cycles as well as the overall phase progression of the tide; while peak amplitudes fall slightly short of the 1.2 m boundary, the deviation is modest and consistent with natural energy attenuation during estuarine propagation, and no artificial amplification or excessive damping is evident, indicating that both second-order schemes yield physically realistic tidal responses throughout the run. The two methods agree closely, as the water-level time series nearly coincide, with only minor, largely inconsequential differences around tidal maxima and minima arising from small amounts of numerical dissipation and dispersion that do not alter the flood–ebb transition, thereby underscoring the numerical consistency, stability, and reliability of MacCormack and Lax–Wendroff for simulating estuarine tidal hydrodynamics under the chosen conditions.

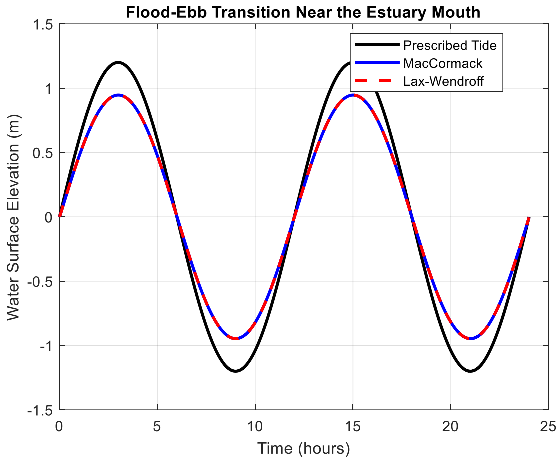

Figure 7. Flood-Ebb Asymmetry at Mid-Estuary

3.3.3 Influence of River Discharge and Tidal Interaction

The interaction between river discharge and tidal forcing significantly controls the hydrodynamic behavior within the Mahakam Estuary. The imposed upstream discharge of 3000 m^3/s counteracts tidal propagation and contributes to tidal damping in the upstream region. The simulations reveal that tidal propagation velocity decreases progressively inland due to the opposing effect of river flow. This interaction also contributes to phase delay and distortion of tidal waveforms along the estuary. The combined influence of tidal forcing and river discharge generates a transitional hydrodynamic regime characterized by bidirectional flow patterns and varying momentum exchange along the estuarine channel.

Table 5. Hydrodynamic Characteristics Predicted by the MacCormack and Lax–Wendroff Schemes

Scheme	Max. Elevation	Min. Elevation	Mean Elevation	Tidal Attenuation
MacCormark	0.94661	-0.94661	8.2935e-07	0.18
Lax-Wendroff	0.94661	-0.94661	8.2935e-07	0.18

Table 5 summarizes the hydrodynamic characteristics obtained from the MacCormack and Lax–Wendroff simulations, including maximum elevation, minimum elevation, mean elevation, and tidal attenuation. Both schemes produced identical maximum and minimum water surface elevations of 0.94661 m and −0.94661 m, respectively, indicating that the two numerical methods generated highly consistent hydrodynamic responses. In addition, the mean elevation values were nearly zero (8.2935×10^{-7}m), suggesting that the simulations are free from any detectable systematic bias or persistent numerical drift over time. Moreover, each of the two schemes yields a consistent tidal attenuation of 0.18 m when compared with the boundary forcing that was prescribed, indicating a modest diminishment of tidal amplitudes as the signal propagates through the estuarine domain. The remarkable concordance between the two numerical solutions underscores their analogous accuracy, stability, and ability to reproduce the tidal dynamics within estuarine environments.

4. CONCLUSION

This study developed a numerical model of tidal hydrodynamics in the Mahakam Estuary using the MacCormack and Lax–Wendroff schemes based on the one-dimensional Saint-Venant equations. This study compared the performance of the MacCormack and Lax–Wendroff schemes for solving the one-dimensional Saint–Venant equations in simulating tidal propagation within the Mahakam Estuary. The results show that both schemes can reproduce key estuarine tidal features, including flood–ebb oscillations, wave propagation, and gradual tidal attenuation under realistic hydrodynamic conditions in the Mahakam Estuary.

The main findings demonstrate that both the MacCormack and Lax–Wendroff schemes successfully reproduce the principal characteristics of tidal hydrodynamics in the Mahakam Estuary, with nearly identical numerical verification metrics and consistent representations of tidal propagation, attenuation, and phase behavior. Although the overall numerical performance of the two schemes is highly comparable, minor differences were observed in their numerical characteristics. The MacCormack scheme tends to generate slightly smoother and more numerically robust solutions under higher CFL conditions, while the Lax–Wendroff scheme preserves somewhat sharper wave propagation features but may introduce small dispersive oscillations near steep flood–ebb transition regions. These differences remained limited and did not significantly affect the overall hydrodynamic predictions. Furthermore, both schemes showed sensitivity to the CFL number and spatial grid resolution, highlighting the importance of appropriate numerical configuration for achieving stable and convergent estuarine simulations.

Overall, the study confirms that both numerical approaches are reliable and suitable for simulating estuarine tidal hydrodynamics in the Mahakam Estuary. Rather than showing substantial performance differences, the findings suggest that each scheme offers modest advantages under specific numerical and hydrodynamic conditions. Consequently, this study provides practical guidance for selecting appropriate finite-difference schemes in estuarine hydrodynamic modeling, particularly for tropical estuarine systems characterized by strong tidal–river interactions and variable bathymetric conditions.

ACKNOWLEDGEMENT

The authors would like to express their sincere gratitude to Politeknik Negeri Balikpapan for providing computational laboratory facilities and technical support during the completion of this research. The availability of the computing resources greatly contributed to the numerical simulations and data analysis conducted in this study.

5. REFERENCES

[1] B. G. Jacob and E. V. Stanev, "Understanding the impact of bathymetric changes in the German Bight on coastal hydrodynamics: One step toward realistic morphodynamic modeling," *Frontiers in Marine Science*, vol. 8, Art. no. 640214, 2021, doi: https://doi.org/10.3389/fmars.2021.640214.

[2] A. C. Fassoni-Andrade *et al.*, "Seasonal to interannual variability of the tide in the Amazon Estuary," *Continental Shelf Research*, vol. 258, Art. no. 104945, 2023, doi: https://doi.org/10.1016/j.csr.2023.104945.

[3] T. Guérin, X. Bertin, and É. Chaumillon, "Wave control on the rhythmic development of a wide estuary mouth sandbank: A process-based modelling study," *Marine Geology*, vol. 381, pp. 44–56, 2016, doi: https://doi.org/10.1016/j.margeo.2016.06.013.

[4] A. B. Fortunato et al., "Sediment dynamics and morphological evolution in the Tagus Estuary inlet," *Marine Geology*, vol. 440, Art. no. 106590, 2021, doi: https://doi.org/10.1016/j.margeo.2021.106590.

[5] P. Bagot, N. Huybrechts, and P. Sergent, "Satellite-derived topography and morphological evolution around Authie macrotidal estuary (France)," *Journal of Marine Science and Engineering*, vol. 9, no. 12, Art. no. 1354, 2021, doi: https://doi.org/10.3390/jmse9121354.

[6] R. Zheng, C. Hu, Z. Sun, and S. Yi-Zhi, "Numerical investigation for the influence of suspended sediment on salinity distribution in the Qiantang Estuary, China," *Frontiers in Marine Science*, vol. 11, Art. no. 1445776, 2024, doi: https://doi.org/10.3389/fmars.2024.1445776.

[7] A. I. Delis and I. K. Nikolos, "Shallow water equations in hydraulics: Modeling, numerics and applications," *Water*, vol. 13, no. 24, Art. no. 3598, 2021, doi: https://doi.org/10.3390/w13243598.

[8] S. Kouhi, M. R. Hashemi, M. L. Spaulding, and T. Hara, "Modeling the impact of sea level rise on maximum water elevation during storm surge events: A closer look at coastal embayments," *Climatic Change*, vol. 172, no. 1–2, Art. no. 25, 2022, doi: https://doi.org/10.1007/s10584-022-03342-x.

[9] M. Deb, A. Abdolali, J. T. Kirby, and F. Shi, "Hydrodynamic modeling of a complex salt marsh system: Importance of channel shoreline and bathymetric resolution," *Coastal Engineering*, vol. 180, Art. no. 104094, 2022, doi: https://doi.org/10.1016/j.coastaleng.2022.104094.

[10] A. M. Alabyan and C. V. Lebedeva, "Flow dynamics in large tidal delta of the Northern Dvina River: 2D simulation," *Journal of Hydroinformatics*, vol. 20, no. 6, pp. 1412–1427, 2018, doi: https://doi.org/10.2166/hydro.2018.051.

[11] Y. Zhang, T. Fernández-Montblanc, W. Pringle, H. Yu, L. Cui, and S. Moghimi, "Global seamless tidal simulation using a 3D unstructured-grid model (SCHISM v5.10.0)," *Geoscientific Model Development*, vol. 16, no. 9, pp. 2565–2589, 2023, doi: https://doi.org/10.5194/gmd-16-2565-2023.

[12] H. Xu, C. D. Cantwell, C. Monteserin, C. Eskilsson, A. P. Engsig-Karup, and S. J. Sherwin, "Spectral/hp element methods: Recent developments, applications, and perspectives," *Archives of Computational Methods in Engineering*, vol. 25, no. 4, pp. 967–1002, 2018, doi: https://doi.org/10.1007/s11831-018-9269-2.

[13] M. Roostaei, A. Nouri, V. Fattahpour, and D. Chan, "Evaluation of numerical schemes for capturing shock waves in modeling proppant transport in fractures," *Journal of Petroleum Exploration and Production Technology*, vol. 7, no. 4, pp. 1097–1110, 2017, doi: https://doi.org/10.1007/s12182-017-0194-x.

[14] E. Ngondiep, A. T. Rubayyi, and J. C. Ntonga, "A MacCormack method for complete shallow water equations with source terms," *arXiv preprint arXiv:1903.11104*, 2019, doi: https://doi.org/10.48550/arXiv.1903.11104.

[15] M. Baccouch, "Numerical methods for the viscid and inviscid Burgers equations," *IntechOpen*, 2024, doi: https://doi.org/10.5772/intechopen.1007351.

[16] L. F. Mateos and M. Hartnett, "Hydrodynamic effects of tidal-stream power extraction for varying turbine operating conditions," *Energies*, vol. 13, no. 12, Art. no. 3240, 2020, doi: https://doi.org/10.3390/en13123240.

[17] X. Chen, "Coupling an unstructured grid three-dimensional model with a laterally averaged two-dimensional model for shallow water hydrodynamics and transport processes," *International Journal for Numerical Methods in Fluids*, vol. 92, no. 11, pp. 1658–1678, 2020, doi: https://doi.org/10.1002/fld.4938.

[18] F. A. Khanza and I. Magdalena, "Numerical model for wave attenuation by breakwater and trench," *Journal of Physics: Conference Series*, vol. 3114, no. 1, Art. no. 012008, 2025, doi: https://doi.org/10.1088/1742-6596/3114/1/012008.

[19] P. Bacigaluppi and M. Kazolea, "Introduction to the special issue on numerical methods and applications for waves in coastal environments," *Water Waves*, vol. 4, no. 3, pp. 307–311, 2022, doi: https://doi.org/10.1007/s42286-022-00071-7.

[20] D. Hu, M. Wang, S. Yao, and Z. Jin, "Study on the spillover of sediment during typical tidal processes in the Yangtze Estuary using a high-resolution numerical model," *Journal of Marine Science and Engineering*, vol. 7, no. 11, Art. no. 390, 2019, doi: https://doi.org/10.3390/jmse7110390.

[21] N. El Assaoui, A. Sadok, A. Bendaraa, and M. M. Charafi, “Two-dimensional numerical modeling of morphodynamic evolution in Bouregreg Estuary (Morocco),” *Archives of Hydro-Engineering and Environmental Mechanics*, vol. 70, no. 2, pp. 103–120, 2023, doi: https://doi.org/10.12912/27197050/166011.
[22] A. Haddach, H. Smaoui, and B. Radi, “La méthode de Boltzmann sur réseaux pour les écoulements côtiers: Application à la lagune de Oualid,” *Open Journal of Modelling and Simulation*, vol. 10, no. 4, pp. 1–15, 2022, doi: https://doi.org/10.21494/iste.op.2022.0867.
[23] L. Casadei, H. Deniau, T. Nodé-Langlois, E. Piot, and C. Polacsek, “Acoustic mode attenuation in ducts (using CFD) with time-domain impedance boundary condition,” *AIAA Journal*, vol. 60, no. 9, pp. 5360–5374, 2022, doi: https://doi.org/10.2514/1.J061879.
[24] H. Xu, C. D. Cantwell, C. Monteserin, C. Eskilsson, A. P. Engsig-Karup, and S. J. Sherwin, “Spectral/hp element methods: Recent developments, applications, and perspectives,” *Archives of Computational Methods in Engineering*, vol. 25, no. 4, pp. 967–1002, 2018, doi: https://doi.org/10.1007/s11831-018-9269-2.
[25] I. García and L. Remaki, “Time-adaptive Adomian decomposition-based numerical scheme for Euler equations,” *Numerical Methods for Partial Differential Equations*, vol. 38, no. 6, pp. 1815–1834, 2022, doi: https://doi.org/10.1002/num.22881.
[26] A. R. Appadu, “Optimized Composite Finite Difference Schemes for Atmospheric Flow Modeling,” *Numerical Methods Partial Differential Eqution*, vol. 35, no. 6, pp. 2171–2192, 2019, doi: 10.1002/num.22407.
[27] [1] K. Lie, "Discretizing Hyperbolic Transport Equations," in *An Introduction to Reservoir Simulation Using MATLAB/GNU Octave*, Cambridge: Cambridge University Press, 2019, pp. 272–288. doi: 10.1017/9781108591416.013.
[28] O. Delestre and P. Lagrée, “A ‘well-balanced’ finite volume scheme for blood flow simulation,” *International Journal for Numerical Methods in Fluids*, vol. 72, no. 2, pp. 177–205, 2012, doi: https://doi.org/10.1002/fld.3736.